Int. J. Electrochem. Sci., 10 **(2015)** 4416 - 4427

International Journal of
ELECTROCHEMICAL
SCIENCE
www.electrochemsci.org

Study on Pitting Corrosion of Storage Tank Bottom Steel in Acidic Condition Using Acoustic Emission

Haisheng Bi, Zili Li[*]*, Jianguo Liu, Yuanpeng Cheng, Isaac Toku-Gyamerah*

College of Pipeline and Civil Engineering, China University of Petroleum, Qingdao, Shandong, 266580, China
[*]E-mail: lizili@upc.edu.cn; haishengbicup@gmail.com

Received: 25 January 2015 / *Accepted:* 28 February 2015 / *Published:* 23 March 2015

The pitting corrosion of atmospheric storage tank (AST) bottom steel specimens was studied by combined using acoustic emission (AE) and electrochemical polarization techniques in acidic NaCl solution. The AE signal characteristic parameters including amplitude, energy, hits, duration time and rise time varied over time, and the relationship between them were analyzed in each stage of pitting corrosion process. The AE parameters and electrochemical polarization curve in time domain were also compared. The result shows that the AE activity is consistent with that of potentiodynamic polarization. The AE signal features are remarkably different in oxidized film rupture, pits propagation and corrosion products movement of the pitting stage. Extracting these AE signal features will be of great help for diagnosing the corrosion severity and identifying the corrosion type of the AE on-line storage tank bottom inspection, and further to assess the corrosion degree of the whole storage tank bottom.

Keywords: Atmospheric storage tank; Pitting corrosion; Acoustic emission; Potentiodynamic polarization; Potentiostatic polarization

1. INTRODUCTION

In petrochemicals industries, corrosion is one of the main causes of catastrophes to structures and equipment. Atmospheric storage tanks, pressure vessels and pipelines are gradually corroded by chemical or electrochemical reactions within their environment. The most common types of corrosion are pitting and uniform corrosion, especially pitting corrosion in low carbon steel. Low carbon steel is widely used as the main material for atmospheric storage tank floors, and the atmospheric storage tanks play an irreplaceable role in storage and transportation of crude oil and oil derivatives. However, over 80% of the storage tanks shutdown, bottom perforation and leakage accidents are caused by tank bottom corrosion. This can cause very serious consequences on the environment, health and safety,

producing a very wide range of hazards and disasters. Therefore, the storage tank bottom corrosion has attracted more and more attentions all over the world in recent decades [1-3].

The corrosion damage of a storage tank bottom is a very complicated process [4, 5]. Several ions such as Na^{+}, Ca^{2+}, $SO4^{2-}$, Cl^{-}, S^{2-}, and dissolved O_2, H_2S, CO_2 in the sedimentary water on tank bottom can induce the corrosion, especially the chloride ions can invade the local deterioration anticorrosion coating and result in pitting corrosion under the coating[6-8], even perforation and leakage. Hence, periodic inspection is necessary to prevent destruction from tank bottom corrosion. Several conventional testing techniques such as magnetic flux leakage (MFL) testing and remote field eddy current testing (RFECT) have been applied to locate and describe the defects [9-12]. However, these techniques require a great deal of process interruption and preparation, for example, opening and cleaning the tank. Therefore, cost-effective and on-line diagnosis techniques are increasingly needed for detecting and evaluating dynamic defects of storage tanks bottom. The acoustic emission method is considered to meet the requirements of an on-line inspection technique and has gained popularity [13-18].

Acoustic emission is a non-destructive technique (NDT), defined by American Society for Testing of Materials (ASTM) as the phenomena whereby transient elastic waves are generated by the rapid release of energy from localized sources within a material, also known as the stress wave emission or micro-seismic activity. It is widely used to monitor process of plastic yield deformation, stress cracking and corrosion damage. Extracting and analyzing the effective signal to evaluate the features of AE sources is the bottleneck to AE on-site inspection. Various researchers have shown that the AE signals are closely related to corrosion factors and electrochemical mechanisms. Fregonese et al. [7] investigated the initiation and propagation stage of pitting corrosion of stainless steel and got hydrogen bubble resonant AE signals in propagation stage. Mansfeld et al. [19] correlated qualitatively pitting corrosion rate of aluminum alloys with AE activity. Similar ideals were also presented in the work of Yuyama and Yamada [20-23]. Darowicki et al. [24, 25] obtained the pitting corrosion potential of aluminum through the cumulative distribution function (CDF) of the probability of pitting corrosion occurrence on the basis of AE data. Alvarez and Lapitz [26-28] results confirmed that the AE activity during the propagation of transgranular stress corrosion cracking (TGSCC) is one order of magnitude higher than the AE activity during the intergranular stress corrosion cracking (IGSCC) propagation. Prateepasen et al. [29-31] assigned AE to hydrogen bubble cavitation and proposed the bubble breakage frequency equation. Lots of AE work had been done focused on pitting corrosion and SCC of the stainless steel and aluminum alloys [32-34]. Nevertheless, very few studies have been carried out on the pitting corrosion of low carbon steel. In that context, the aim of the present study is to give the characteristic of AE signals during pitting corrosion of storage tank bottom steel.

2. EXPERIMENTAN PROCEDURE

2.1. Material

Specimens were cut into small squares using wire-electrode cutting method and their sizes are 2.9 by 2.9 by 0.2 cm^3. Composition of steel is given in Table 1. The exposed surface was polished with

a series of silicon carbide sheets of up to 1200 grit. The specimens were rinsed with de-ionized (DI) water then acetone and alcohol, after that they were dried in a desiccator, and weighed, labeled and stored to be used.

Table 1. Composition of the studied material

Element	Fe	C	Si	Mn	P	S
Wt.%	Balance	0.17	0.3	0.61	0.05	0.045

2.2. Experimental device

The experiments were conducted in a 3.0 wt. % NaCl solution with pH adjusted to 2.0 with the addition of hydrochloric acid (HCl) at room temperature. The size of the electrolytic cell is 25 by 25 by 25 cm^3, and it is made of transparent organic glass to avoid producing other corrosion signal. A small plate with 4×Φ9 mm round holes at the bottom was used to separate the work electrode and reference electrode, and to eliminate the hydrogen bubble signal interference. The specimen was sealed by epoxy resin and inserted in the center stepped hole of the electrolytic cell bottom, and the edges of the hole were filled with silicone sealant to ensure no leakage (see Figure 1). An AE sensor was mounted on the back of the specimen for real-time monitoring corrosion signals and connected to the AMSY-5 data acquisition channel through a coaxial cable. The electrochemical measurements were conducted simultaneously to confirm the result of acoustic emission detection.

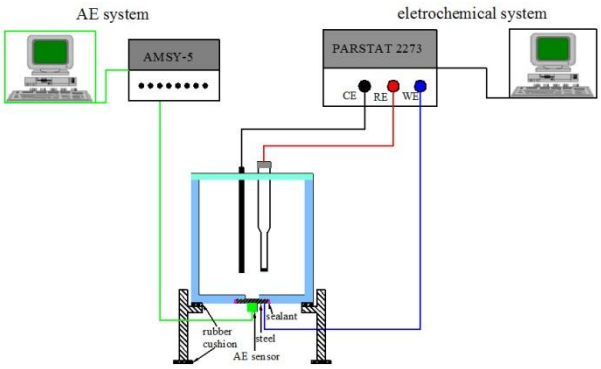

Figure 1. Schematic diagram of experiment system

2.3. Electrochemical device

Electrochemical measurements were carried out with a PAR 2273 electrochemical workstation produced by AMETEX. The minimum current resolution of system is 1.2 fA and the minimum potential step is 2.5 μV. A typical three-electrode system was set up. The sample used as the working electrode (WE), its electrochemical potential was measured with a saturated calomel (SCE) reference electrode (RE) and a platinum plate as the counter electrode (CE).

2.4. Acoustic Emission monitoring

AE instrumentation consisted of a piezoelectric sensor (VS150-RIC type from Vallen, integral preamplifier: 34 dB gain) and an acquisition device AMSY-5 from Germany Vallen Systeme GmbH, the AMSY-5 was a fully digital multi-channel AE measurement system to extract AE parameters. The frequency response curve of the sensor was shown in Figure 2. AE acquisition threshold was fixed at 30.2 dB according to background noise level and filtered by band pass from 25 to 850 kHz.

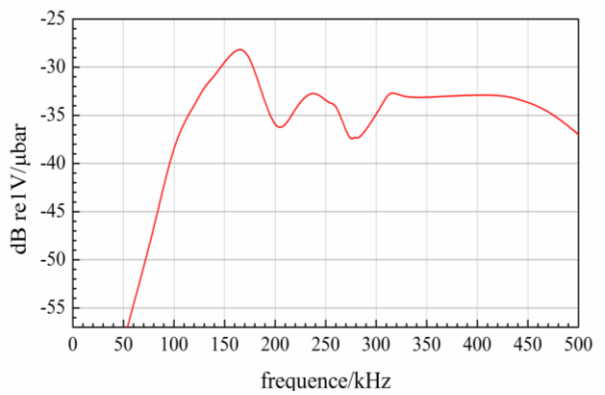

Figure 2. Frequency response curve of the AE sensor

3. RESULTS AND DISCUSSION

The corrosive solution was filled into a glass cell at 80% of the container's height, standing for about 2 hours until the solution become stable. Then the open circuit potential (OCP) was measured and the curve was shown in Figure 3.

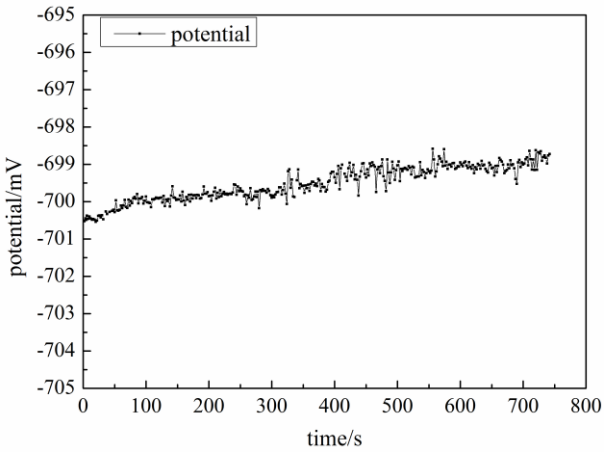

Figure 3. Open circuit potential decay curves for low carbon steel in 3% NaCl solution at pH 2.0

The change of OCP was less than 1 mV over 10 minutes, which indicated that the corrosion system had reached a relatively stable status. The result of an electrochemical corrosion process of the

carbon steel is shown below. The corrosion process of metal comprises an oxidation and reduction reaction.

Anodic reaction: $Fe \rightarrow Fe^{2+} + 2e^{-}$ (1)

The ferrous ions are not stable and get rapidly oxidized to ferric ions as follows:

$Fe^{2+} \rightarrow Fe^{3+} + e^{-}$ (2)

Cathodic reaction: $2H^{+} + 2e^{-} \rightarrow H_2$ (3)

$O_2 + 4H^{+} + 4e^{-} \rightarrow 2H_2O$ (4)

Overall reaction: $(Fe^{3+} + 3Cl^{-}) + 3H_2O \rightarrow Fe(OH)_3 + 3H^{+} + 3Cl^{-}$ (5)

The chloride ions are absorbed on the materials surface and invade the local defect of the passive film, further break the film, and these reactions could lead to the formation of $FeCl_2$ and $FeCl_3$ which can migrate continuously from the interface to the solution.

AE monitoring was conducted simultaneously to acquire and store data. In the accelerated corrosion process, the exfoliation and rupture of oxidized film invaded by chloride ion, the deposits and friction of corrosion products could also generate obvious AE signals.

3.1 AE signal features under potentiodynamic polarization

The potentiodynamic polarization scanned on the range of -0.25V (vs.OCP) ~1.60V with a scan rate of 0.50mV/s, and the AE data was acquired simultaneously. The potentiodynamic polarization curve was showed in Figure 4. When the specimen was polarized to a high potential, the surface of the specimen began to oxidize and a very thin anodic oxide film was formed. The current density reduced significantly for the membrane resistance when potential reached 0.3V level. In this stage, the new anodic oxide film formation rate was higher than the old film dissolution rate. As a result, the whole metal surface was gradually covered by the oxide film, and the thickness of oxide film increased with the time. With the increase of potential, the active chlorine ions adsorbed and gathered on the surface of localized oxide film defects. The chlorine ions intensively invaded localized defects and accelerated greatly the film dissolution. The film was destroyed locally and the metal matrix exposed to form an active dissolution point. The small dissolution was named as pitting nuclear. The oxide film of low carbon steel breakage was observed between the potential 0.8~1.0V through potentiodynamic polarization experiments.

The AE hits distribution with time presented four stages corresponding to potentiodynamic polarization curve above, the AE hits showed fairly good consistency with the later, the I, II, III and IV stages were shown in Figure 5. In the stage I, there was very few AE signals be observed, for the metal just began to dissolve and the rate of surface oxide film formation was relatively small. Both AE intensity and AE activity were at low level from 500 to 2000s. AE signals began to increase sharply in the stage II, most of the AE signal generated by the film formation and film dissolution behaviors, and the new film formation gradually became dominant. It showed that the average hits rate increased rapidly to 1.2 hits/s.

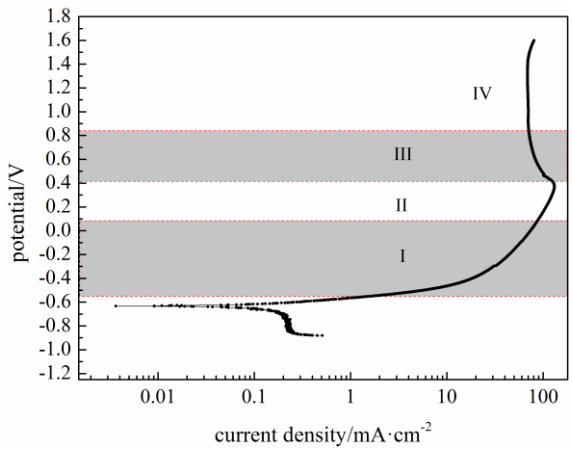

Figure 4. Potentiodynamic polarization curve at scanning rate 0.5 mV/s of low carbon steel in 3% NaCl solution at pH 2.0

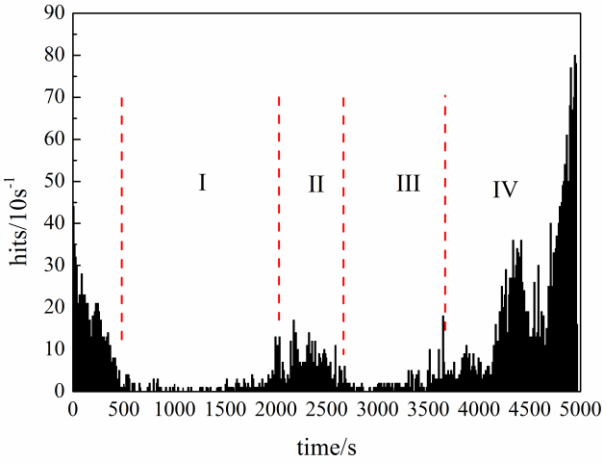

Figure 5. AE hits distribution with time (/10s)

The AE signal amplitude distribution with time was shown in Figure 6. From 2000 to 2700s, the AE amplitude mainly distributed from 32 to 45dB, AE intensity was much stronger than the stage I. From 2700 to 3600s, AE signals decreased significantly, and both AE intensity and AE activity were much lower than the stage II. It was indicated that the oxide film had covered all metal surface in this stage. The oxide film separated the metal matrix from corrosion solution and hindered the metal ions from directly going into the solution. About 3600s later, AE activity increased sharply, the biggest AE hits rate had reached 8 hits/s. Meanwhile, AE intensity also increased, the maximum AE amplitude was up to 60 dB. AE signal was more intensive and stronger than the first three stages. The results showed that the oxide film exfoliated from metal matrix and ruptured, the pitting nuclear grew to be many visual pits and the corrosion products cumulated in the vicinity of the pits. These pits then developed as occluded cells with the formation of a metallic cap at a sufficient rate. The hydrolysis of Fe^{3+} ions inside the occluded cells elevated the local H^{+} concentration, and the migration of Cl^{-} ions

and the formation of H^+ ions made the cells more acidic. The occluded cells were kept in an active state and the pits grew deeper.

As shown in Figure 7, in the final stage of polarization test, lots of high amplitude AE signals emerged. The signal amplitude is over 50 dB and the duration time is less than 80μs. It further illustrates the pitting corrosion is in a high active state in this stage.

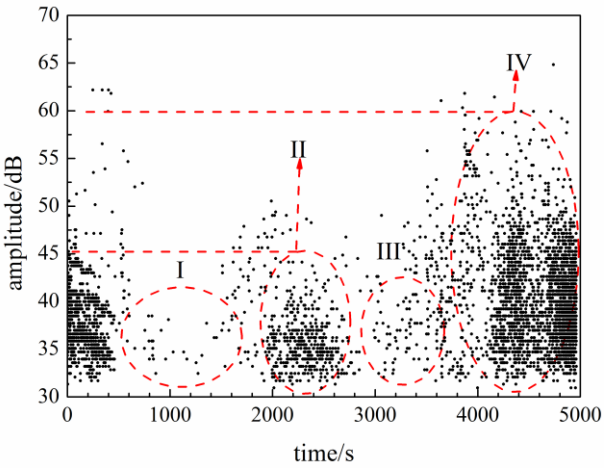

Figure 6. AE signal amplitude distribution with time under potentiodynamic polarization

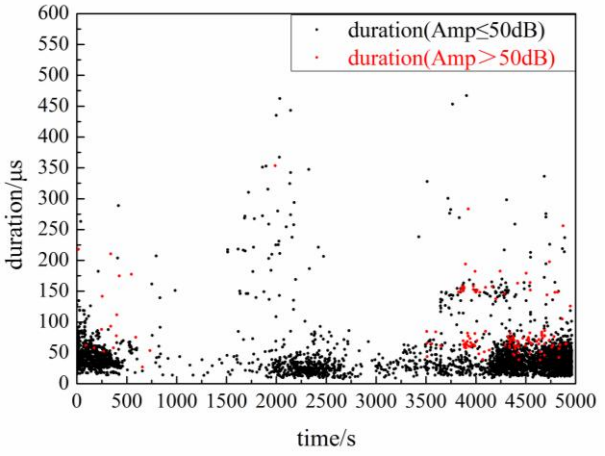

Figure 7. AE hits duration distribution with time under potentiodynamic polarization

3.2 AE signal features under potentiostatic polarization

According to the potentiodynamic polarization curve, the potential was kept at 1.0V by a potentiostat to keep stable pitting corrosion on the specimen. The potentiostatic polarization test lasted 2 hours, and acquired the AE signals simultaneously. As shown in Figure 8, a large number of AE signals can be detected throughout the whole corrosion process, the AE activity and AE intensity were at a very high level. Especially in the time region of 900~1200s and after 3600s, both the AE activity and AE intensity increased significantly, some AE signals amplitude even exceed 65 dB, and the high duration signals over 100μs emerged frequently in the two time regions. From 900 to 1200s, the

exfoliation, shrinking and breakage of the oxide film generated rich AE signals, accompanied with the high duration signals. After the rupture of the oxide film, the AE activity decreased relatively, pitting corrosion was in the initiation stage, also named as induction period. After 3200s, The AE activity and intensity increased again, it illustrated that the corrosion products began to exfoliate, the friction and cracking in corrosion products layers resulted in rich high duration signals. The AE hits correlation with amplitude showed that AE amplitude mainly ranged from35 to 45dB in Figure 9, and distributed throughout the whole acquisition time.

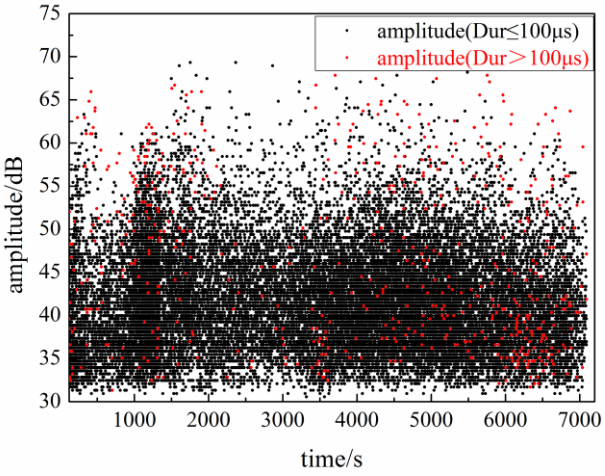

Figure 8. AE signal amplitude distribution with time under potentiostatic polarization

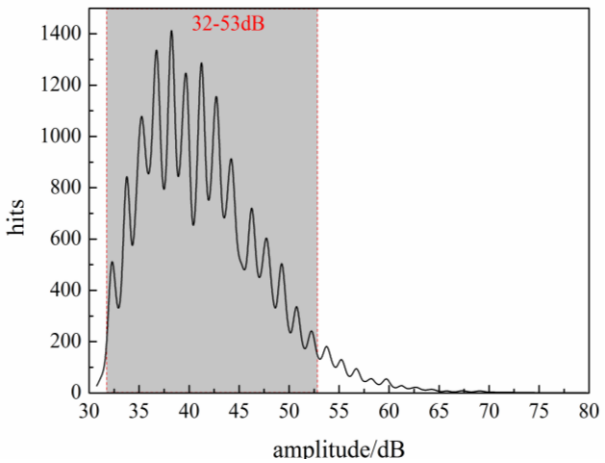

Figure 9. AE hits correlation with amplitude

To further confirm the features of the AE signal during the pitting corrosion process, correlation analysis among AE hits, energy and duration was shown in Figure 10 and Figure 11. The AE hits main peak value corresponding to the signal duration was 35~55μs, it can be seen that the second hits peak was 150~170μs by amplifying part of the graph in Figure 10. The AE signal energy main peak value corresponding to the signal duration was 50~80μs, the second energy peak was about

160~180μs. Comparing the two Figures, the duration of AE hits two peaks were not coincident with AE energy two peaks. This feature further illustrated that, among the AE signals generated by pitting corrosion, the high energy signals have a relatively high duration. The occurrence of the main and second peak showed that the majority of AE hits was generated by pits growth and propagation, these signals had a relatively short duration time, while AE hits released from oxide film rupture took up a small part, but the signal energy and duration were relative higher, which resulted in a slight migration of the energy peak towards the longer duration. This conclusion is coincident with the results acquired by Parteepasen and Jirarungsatian [29, 35]. However, in their study, they didn't analyze the correlations between AE hits and duration, and correlations between AE energy and duration. AE hits and energy most directly reflect the activity of the AE source, the AE energy changes really reflect the energy released from local corrosion activity, these can be helpful for recognizing the different corrosion behaviors. Figure 10 and Figure 11 further confirmed that these two kinds of signals were mainly generated by pits growth and films breakage respectively.

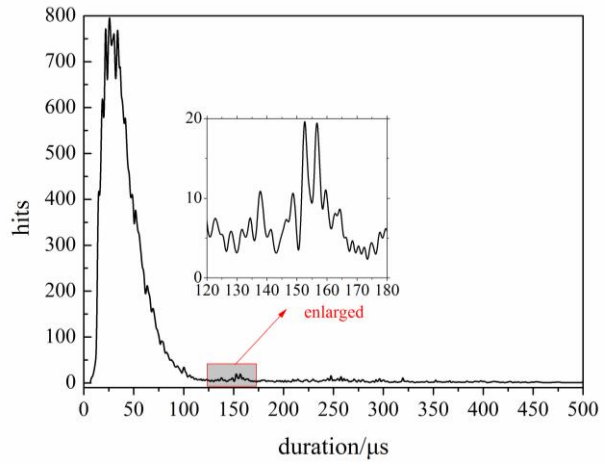

Figure 10. AE hits correlation with duration

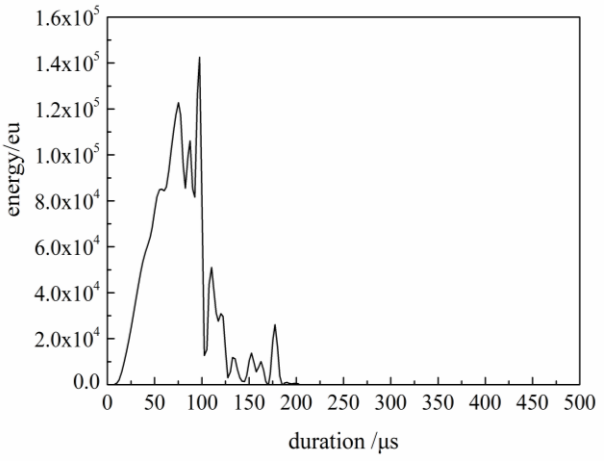

Figure 11. AE energy correlation with duration (1eu=10^{-14} V^2s)

Based on the above analysis, there are three typical AE sources in pitting corrosion: exfoliation and rupture of the oxide film, the growth and propagation of the pits, friction and cracking in corrosion products layers. The clustering analysis of the AE sources was shown in Figure 12. It showed that the relatively long duration signals were released from oxide film rupture and corrosion products activities. A large number of dominant AE signals with short duration were generated by pits growth and propagation.

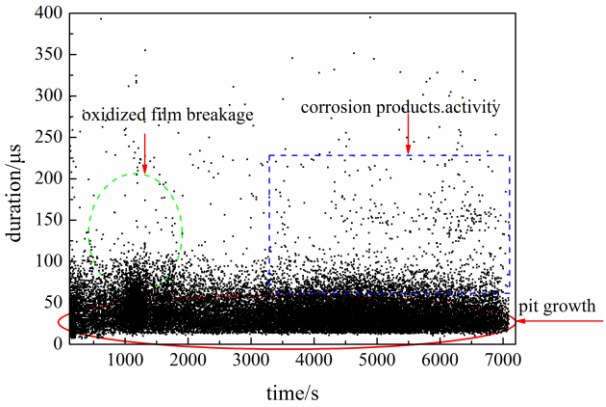

Figure 12. AE hits duration distribution with time under potentiostatic polarization

The result is confirmed by the observation of the pits at the end of the test using Zeiss Axio 3D confocal metallographic microscope, the sample surface morphology and pits image were shown in Figure 13. The 3D surface topography characterized the morphology and the size of the pits. A large number of honeycomb pits distributed on the surface of specimen, and most of the pits depth was on an average of 250 μm by the statistical analysis, which further confirmed that the specimen surface was indeed undergoing severe pitting corrosion.

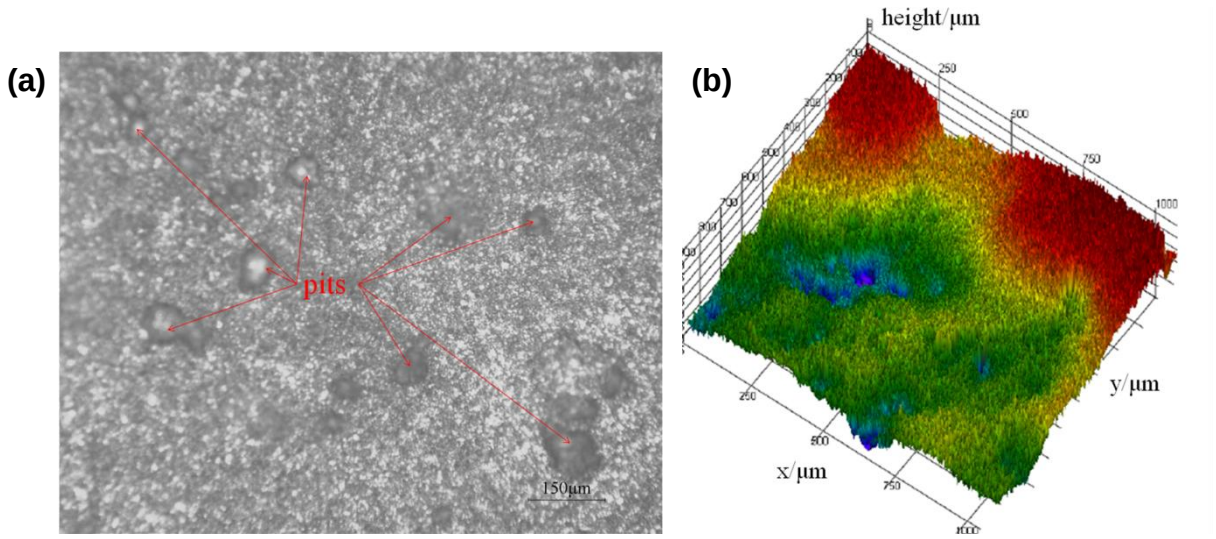

Figure 13. Surface morphology of specimen after potentiostatic test 2 hours in 3% NaCl solution at pH2.0 (a) surface morphology (×100) and (b) 3D pits image (×200)

4. CONCLUSIONS

This work aimed at studying pitting corrosion of storage tank bottom steel using the AE method, and the following conclusions can be obtained:

1. Pitting corrosion of storage tank bottom steel can generate rich acoustic emission. And the AE monitoring results have a good consistency with the electrochemical testing results. The AE signal features can describe each stage of pitting corrosion well.

2. After elimination the interference of hydrogen bubbles burst signal, the exfoliation and rupture of the oxide film, pits growth and propagation, piling up of corrosion products, friction and cracking in corrosion products layers are the main AE source. Pits growth AE signal duration is less than 80 μs, while oxide film rupture and the friction in the corrosion products layer signal duration is concentrated in 130 ~ 170μs.

3. The AE signal amplitude in the storage tank bottom steel pitting is almost lower than 65 dB, and is concentrated from 32 to53 dB. AE signal amplitude from oxide film breakage and corrosion products cracking is a little higher. It will be of great help for diagnosing the corrosion severity and identifying the corrosion type of the AE on-line storage tank floor inspection, and further to assess the corrosion degree of the whole tank bottom.

ACKNOWLEDGEMENTS
The authors greatly acknowledge the financial support provided by the Projects of National Natural Science Foundation of China (51301201) and Shandong Provincial Natural Science Foundation, China (ZR2013EMQ014). We also wish to express our gratitude to the Shengli Oilfield Technical Test Center, Sinopec, China for AMSY-5 device.

Reference

1. J. Shuai, K. Han and X. Xu, *J. Loss. Prevent. Proc.*, 25 (2012) 166
2. F. Liu, X. Guo, D. Hu, W. Guo and N. Jin, *Nondestruct. Test. Eva.*, 25 (2010) 45
3. J.X. Zhu, *Journal of Materials Protection*, 42 (2009) 56
4. Y. Zhou, M. Liu, X. Ni, D. Chen and W. Wei, *Advanced Materials Research*, 317 (2011) 66
5. A. Zagorski, H. Matysiak, O. Tsyrulnyk, O. Zvirko, H. Nykyforchyn and K. Kurzydlowski, *Mater. Sci.*, 40 (2004) 421
6. M. Fregonese, L. Jaubert and Y. Cetre, *Prog. Org. Coat.*, 59 (2007) 239
7. M. Fregonese, H. Idrissi, H. Mazille, L. Renaud and Y. Cetre, *Corros. Sci.*, 43 (2001) 627
8. X. Zhao and J. Jiang, *China Safety Science Journal*, 15 (2005) 104
9. C. Jomdecha, A. Prateepasen and P. Kaewtrakulpong, *NDT & E Int.*, 40 (2007) 584
10. A.R. Ramirez, J.S.D. Mason and N. Pearson, *NDT & E Int.*, 42 (2009) 16
11. N. Kasai, Y. Fujiwara, K. Sekine and T. Sakamoto, *NDT & E Int.*, 41 (2008) 525
12. N. Kasai, K. Sekine and H. Maruyama, *Journal of the Japan Petroleum Institute*, 47 (2004) 19
13. J.F. Chen, H.S. Bi, Q. Wang, A.Q. Wang, H. Sheng and H.X. Rong, *Advanced Materials Research*, 807 (2013) 2652
14. H.S. Bi, Z.L. Li, Y.P. Cheng, Isaac and J. Wang, *Advanced Materials Research*, 694 (2013) 1167
15. M. Riahi, H. Shamekh and B. Khosrowzadeh, *Russ. J. Nondestruct*, 44 (2008) 436
16. M. Riahi and H. Shamekh, *Russ. J. Nondestruct*, 42 (2006) 537
17. A.V. Sokolkin, I.Y. Ievlev and S.O. Cholakh, *Russ. J. Nondestruct,* 38 (2002) 113

18. A.V. Sokolkin, I.Y. Ievlev and S.O. Cholakh, *Russ. J. Nondestruct,* 38 (2002) 902
19. A.M. Reyman, E.V. Krotov and A.D. Mansfeld, *Proceedings of the Society of Photo-Optical Instrumentation Engineers*, 2 (2001) 109
20. S. Park, S. Kitsukawa, K. Katoh, S. Yuyama, H. Maruyama and K. Sekine, *Mater. Trans.*, 46 (2005) 2490
21. N. Kasai, K. Utatsu, S. Park, S. Kitsukawa and K. Sekine, *Corros. Sci.*, 51 (2009) 1679
22. S. Park, S. Kitsukawa, K. Katoh, S. Yuyama, H. Maruyama and K. Sekine, *Mater. Trans.*, 47 (2006) 1240
23. S. Yuyama, M. Yamada, K. Sekine and S. Kitsukawa, *Mater. Eval.*, 65 (2007) 888
24. K. Darowicki, J. Orlikowski, A. Arutunow and W. Jurczak, *J. Electrochem. Soc.*, 154 (2007) C74
25. S. Krakowiak and K. Darowicki, *J. Solid State Electr.*, 13 (2009) 1653
26. P. Lapitz, J. Ruzzante and M. Alvarez, *Corros. Sci.*, 49 (2007) 3812
27. M. Alvarez, P. Lapitz and J. Ruzzante, *Corros. Sci.*, 50 (2008) 3382
28. M. Alvarez, P. Lapitz and J. Ruzzante, *Corros. Sci.*, 55 (2012) 5
29. A. Prateepasen and C. Jirarungsatian, *Corrosion*, 67 (2011) 056001
30. C. Jirarungsatian and A. Prateepasen, *Corros. Sci.*, 52 (2010) 187
31. A. Prateepasen, P. Kaewtrakulpong and C. Jirarungsatean, *Advanced Nondestructuve Evaluation*, 321-323 (2006) 549
32. M. Boinet, J. Bernard, M. Chatenet, F. Dalard and S. Maximovitch, *Electrochim. Acta*, 55 (2010) 3454
33. H. Leinonen, T. Schildt, H. Hanninen, *Metallurgical and Materials Transactions a-Physical Metallurgy and Materials Science*, 42A (2011) 424
34. V. Smanio, M. Fregonese, J. Kittel, T. Cassagne and B. Normand, *Corros. Sci.*,53 (2011) 3942
35. A. Prateepasen, C. Jirarungsatean and P. Tuengsook, *Advanced Nondestructuve Evaluation*, 321-323 (2006) 545